

Variational compilation of native gates for efficient trapped-ion Hamiltonian simulation

Peng Wang(王鹏), Chunyan Li(李春燕), Hao Shi(石皓), Ping-Xing Chen(陈平形)

Citation: Chin. Phys. B. 35, 090305 (2026). DOI: 10.1088/1674-1056/ae6b33 | CSTR: 32038.14.CPB.ae6b33
http://cpb.iphy.ac.cn; http://iopscience.iop.org/cpb

What follows is a list of articles you may be interested in

Robust quantum gate optimization with first-order derivatives of ion–phonon and ion–ion couplings in trapped ions

Jing-Bo Wang(汪景波)
Chin. Phys. B. 34, 040302 (2025). DOI: 10.1088/1674-1056/adb40e | CSTR: 32038.14.CPB.adb40e

M2CS: A microwave measurement and control system for large-scale superconducting quantum processors

Jiawei Zhang(张家蔚), Xuandong Sun(孙炫东), Zechen Guo(郭泽臣), Yuefeng Yuan(袁跃峰), Yubin Zhang(张玉斌), Ji Chu(储继), Wenhui Huang(黄文辉), Yongqi Liang(梁咏棋), Jiawei Qiu(邱嘉威), Daxiong Sun(孙大雄), Ziyu Tao(陶子予), Jiajian Zhang(张家健), Weijie Guo(郭伟杰), Ji Jiang(蒋骥), Xiayu Linpeng(林彭夏雨), Yang Liu(刘阳), Wenhui Ren(任文慧), Jingjing Niu(牛晶晶), Youpeng Zhong(钟有鹏), Dapeng Yu(俞大鹏)
Chin. Phys. B. 33, 120309 (2024). DOI: 10.1088/1674-1056/ad8a49

Dynamical nonlinear excitations induced by interaction quench in a two-dimensional box-trapped Bose–Einstein condensate

Zhen-Xia Niu(牛真霞), Chao Gao(高超)
Chin. Phys. B. 33, 020314 (2024). DOI: 10.1088/1674-1056/ad1179

Nonlinear modes coupling of trapped spin–orbit coupled spin-1 Bose–Einstein condensates

Jie Wang(王杰), Jun-Cheng Liang(梁俊成), Zi-Fa Yu(鱼自发), An-Qing Zhang(张安庆), Ai-Xia Zhang(张爱霞), Ju-Kui Xue(薛具奎)
Chin. Phys. B. 32, 090305 (2023). DOI: 10.1088/1674-1056/accd53

Achieving ultracold Bose-Fermi mixture of 87Rb and 40K with dual dark magnetic-optical-trap

Jie Miao(苗杰), Guoqi Bian(边国旗), Biao Shan(单标), Liangchao Chen(陈良超), Zengming Meng(孟增明), Pengjun Wang(王鹏军), Lianghui Huang(黄良辉), Jing Zhang(张靖)
Chin. Phys. B. 31, 080306 (2022). DOI: 10.1088/1674-1056/ac5882

Variational compilation of native gates for efficient trapped-ion Hamiltonian simulation

Peng Wang(王鹏)[1], Chunyan Li(李春燕)[1], Hao Shi(石皓)[2], and Ping-Xing Chen(陈平形)[1,†]

[1] *College of Science, National University of Defense Technology, Changsha* 410073, *China*
[2] *College of Intelligence Science and Technology, National University of Defense Technology, Changsha* 410073, *China*

(Received 26 February 2026; revised manuscript received 16 April 2026; accepted manuscript online 11 May 2026)

Quantum simulation on noisy intermediate-scale quantum (NISQ) hardware is limited by short coherence time and gate errors. We present a universal variational compilation optimization method (VCOM) that directly leverages the native gate set of trapped-ion processors, namely single-qubit rotations and global Ising-type XX interactions, to construct shallow circuits for simulating molecular Hamiltonians. Specifically, VCOM employs a hybrid optimization strategy combining genetic algorithms with gradient-based refinement to compile Pauli string evolution operators e^{-iPt}, thereby substantially reducing circuit depth and multi-qubit gate overhead in Hamiltonian simulation. Applied to hydrogen chains, the compiled circuits achieve fidelities comparable to standard decompositions while reducing the proportion of two-qubit operations to only 1.9%–4.6% of the total native gates, a significant improvement over the standard second-order Trotter–Suzuki product formula. Under experimentally motivated laser-intensity and phase-noise models, the proposed scheme maintains high fidelity and exhibits significantly slower degradation than direct native gate decompositions of conventional circuits. These results establish native-gate-based variational compilation as a scalable and practical approach for digital quantum simulation on trapped-ion platforms, with potential extensions to strongly correlated systems and non-equilibrium dynamics.

Keywords: variational compilation, trapped-ion quantum computing, molecular Hamiltonian simulation

PACS: 03.67.Ac, 03.67.Lx, 37.10.Ty

DOI: 10.1088/1674-1056/ae6b33 **CSTR:** 32038.14.CPB.ae6b33

1. Introduction

Quantum computing offers the prospect of exponential speedups for tasks such as integer factorization[1] and the simulation of quantum systems.[2] However, realizing these advantages generally requires fully fault-tolerant architectures. Current quantum processors fall into the category of noisy intermediate-scale quantum (NISQ) hardware,[3] which remains limited by qubit number, connectivity, and intrinsic noise. These constraints impose stringent bounds on the feasible depth of quantum circuits. To enable practical applications within the coherence times of NISQ hardware, it is essential to translate quantum algorithms into low-error sequences of physical operations — a process known as quantum compilation.

In the NISQ era, the objective of quantum compilation has shifted from ensuring universality toward minimizing the use of costly and error-prone operations, particularly multi-qubit gates, thereby enabling quantum algorithms to complete execution before accumulated noise dominates the outcome. Multi-qubit gates typically require complex interactions among several qubits, which result in higher error rates and reduced computational accuracy. By contrast, single-qubit gates generally achieve much higher fidelities due to their relative simplicity of implementation. To address these challenges, a variety of methods for gate synthesis and quantum algorithm compilation have been developed,[4–9] including methods inspired by machine learning,[10,11] such as reinforcement learning,[12–14] as well as automated planning techniques.[15] These strategies aim to improve the efficiency of quantum circuit compilation and mitigate the intrinsic limitations of current quantum hardware.

Beyond conventional approaches, a promising paradigm is to employ quantum processors themselves to train parameterized quantum circuits, known as variational quantum algorithms (VQAs),[16–19] which provide a novel framework for quantum compilation. Using the Hamiltonian variational technique[20,21] to design a shallow and trainable ansatz has enormous potential and can greatly minimize the number of gates. In addition, the grouping design of Clifford circuits can utilize commuting groups[22,23] to construct more streamlined and efficient parameterized quantum circuits, further reducing the consumption of quantum gates. However, as the scale of the simulation system increases, the number of optimized parameters required for the Hamiltonian variational ansatz (HVA) rapidly increases, which presents scalability challenges and performs poorly when dealing with Hamiltonian quantities with long-range interactions. By designing predefined templates with specific gate sets and using quantum-assisted compilation techniques,[24–27] circuit depth can be reduced and algorithm efficiency can be improved. However,

†Corresponding author. E-mail: pxchen@nudt.edu.cn

© 2026 Chinese Physical Society and IOP Publishing Ltd. All rights, including for text and data mining, AI training, and similar technologies, are reserved.

the majority of these methods rely on superconducting quantum gate sets for optimization or decomposition, and have primarily been validated on superconducting hardware. Although superconducting platforms currently dominate VQA research, trapped-ion architectures offer distinct advantages that may enable more efficient and noise-resilient compilation.

The trapped-ion system[28–33] is one of the leading candidates for large-scale quantum computing due to its long coherence times and high-fidelity gate operations. Unlike superconducting architectures, which are typically restricted to nearest-neighbor couplings, trapped-ion platforms feature all-to-all connectivity mediated by collective motional modes, thereby eliminating the need for SWAP operations and reducing compilation overhead. Solving for the molecular ground state energy using VQA with the unitary coupled cluster singles and doubles (UCCSD) ansatz has been verified many times in trapped-ion systems.[34–37] To achieve this on current hardware, researchers strike a balance between implementation accuracy and circuit depth by choosing a smaller active space and primary excitation operators,[34] or by reducing resource requirements through a collaborative design framework that co-optimizes the algorithm and the trapped-ion hardware.[35] This includes using full connectivity to avoid SWAP gates, simplifying circuits for boson terms, and carefully sequencing the order of multiple excitation operators to reduce the number of CNOT gates. In linear ion traps,[38] fully connected interactions can be realized without additional qubit scheduling, which substantially shortens algorithm runtime and provides a distinct performance advantage. An important research direction is to recompile quantum circuits directly into the native gate set of trapped-ion devices, enabling efficient Hamiltonian simulation. Global connectivity and high-fidelity operations are key hardware characteristics of trapped ions that offer a promising foundation for resource-efficient quantum compilation.

In this work, we propose a universal variational compilation optimization method (VCOM) specifically designed for Hamiltonian simulation on trapped-ion systems. Unlike conventional decomposition methods, our method directly employs native trapped-ion gates, specifically single-qubit rotations $(R_X(\theta), R_Y(\theta))$ and multi-qubit entangling gates (Ising-type $XX(\theta)$ and global Ising-type $GXX(\theta)$), to directly compile Pauli-string evolution operators using a hardware-efficient approach. The core of VCOM lies in a robust hybrid optimization strategy, where a genetic algorithm performs a global search to identify promising parameters, which are then refined by gradient-based methods, all while dynamically pruning redundant gates to achieve shallow, efficient circuits. Through simulations of H_2, H_3, and H_4 molecular Hamiltonians using the second-order Trotter–Suzuki product formula, the results demonstrate that VCOM not only achieves fidelities exceeding 99.5% but also drastically reduces the proportion of two-qubit gates to a mere 1.9%–4.6% of the total gate count, a marked improvement that directly translates to lower resource demands. Furthermore, we incorporate realistic noise models, including laser intensity and phase noise, and demonstrate that the proposed scheme maintains strong noise resilience under such conditions. These findings collectively establish the effectiveness and noise tolerance of VCOM. VCOM can not only precisely simulate molecular energies but also address more complex problems such as strongly correlated materials and non-equilibrium quantum dynamics on near-term trapped-ion processors.

2. Resource-efficient native-gate compilation for molecular Hamiltonian simulation

2.1. Native gate set of trapped-ion processors

Trapped-ion quantum processors offer several key advantages for efficient quantum compilation, including all-to-all connectivity mediated by shared motional modes and high-fidelity gate operations. These features mitigate the SWAP overhead commonly encountered in superconducting quantum architectures. Additionally, trapped-ion systems feature a well-defined native gate set that serves as a foundation for digital quantum simulation. Single-qubit rotations around the x, y, and z axes $(R_X(\theta), R_Y(\theta), R_Z(\theta))$ can be implemented with high fidelity using resonant laser pulses. Multi-qubit entangling operations are realized through Ising-type interactions, most notably the Mølmer–Sørensen (MS) gate,[39,40] which corresponds to an XX coupling between qubits. Beyond pairwise XX interactions, trapped-ion systems support global XX interactions that simultaneously couple all qubits, a unique capability not found in most other quantum architectures. Collectively, these native operations form a versatile and experimentally accessible gate set, making trapped-ion systems particularly well-suited for quantum algorithms and Hamiltonian simulation. However, to achieve these functions, traditional compilation methods are required to decompose logical gates into native gate sequences, a process that incurs additional overhead. In contrast, directly compiling into the native gate set bypasses this intermediate decomposition step, thereby reducing circuit depth and multi-qubit gate count and enabling efficient implementation of these functions.

In trapped-ion systems, lasers play an indispensable role in ion trapping, ion cooling, as well as quantum state manipulation and detection. The interaction between lasers and ions is realized by tuning the laser frequency to different ionic energy levels, including carrier resonance excitation, red sideband excitation, and blue sideband excitation. These processes involve the coupling between the internal electronic states of the ions and their motional (phonon) states, which directly affects the

quantum state evolution of the ions. When the ions undergo harmonic oscillations around their equilibrium positions in the trap, two long-lived energy levels are typically chosen to form a two-level system, which can be treated as a qubit. When an external laser is resonant with the ionic energy levels, the interaction Hamiltonian between the ion and the laser can be expressed as

$$\begin{aligned} H &= H_0 + H_{\rm I}, \\ H_0 &= \sum_{i=1}^{3} \frac{p_i^2}{2m} + \frac{1}{2} m\omega_i^2 x_i^2 + \frac{1}{2}\hbar\omega_0\sigma_z, \\ H_{\rm I} &= \frac{1}{2}\hbar\Omega\left(\sigma^+ + \sigma^-\right) \\ &\quad \times \left(\mathrm{e}^{\mathrm{i}(kx_i+\omega_{\rm l}t+\phi)} + \mathrm{e}^{-\mathrm{i}(kx_i+\omega_{\rm l}t+\phi)}\right). \end{aligned} \tag{1}$$

Here, p_i represents the momentum of the ion, x_i represents its coordinate, ω_0 is the angular frequency of the transition between the two levels, k is the wave vector of the laser, $\omega_{\rm l}$ is the laser frequency, and ϕ is the initial phase of the laser. σ_z is the Pauli-Z operator, and $\sigma_\pm = (\sigma_x \pm \mathrm{i}\sigma_y)/2$ are the ladder operators acting on the qubit. H_0 represents the Hamiltonian of the ion itself, while $H_{\rm I}$ denotes the interaction Hamiltonian between the ion and the laser, with the coupling strength given by the Rabi frequency Ω.

The ion's position is described using creation and annihilation operators, and we adopt the laser rotating frame. Consider the case where the motional wavepacket of the ion is much smaller than the laser wavelength. This condition defines the Lamb–Dicke regime. Under this regime, the interaction Hamiltonian can be further simplified using the rotating-wave approximation, yielding

$$\begin{aligned} H_{\rm I}' &= \frac{\hbar}{2}\Delta\sigma_z + \frac{\hbar}{2}\Omega\{\sigma^+\mathrm{e}^{\mathrm{i}\phi}[1 + \mathrm{i}\eta_i(a_i\mathrm{e}^{-\mathrm{i}\omega_i t} \\ &\quad + a_i^\dagger \mathrm{e}^{\mathrm{i}\omega_i t})] + \mathrm{h.c.}\}. \end{aligned} \tag{2}$$

Here, Ω is the Rabi frequency when the mean phonon number is zero. If the Rabi frequency satisfies $\Omega \ll \omega_i$, the interaction Hamiltonian can again be simplified using the rotating-wave approximation, enabling resolved sideband operations on the ions. Depending on the change in the phonon number, the coupling between the ion and the laser can be classified into carrier transitions, red-sideband transitions, and blue-sideband transitions.

Single-qubit gates can be implemented via carrier transitions. When the detuning is zero, the system undergoes coherent conversion between $|\uparrow\rangle$ and $|\downarrow\rangle$, and the corresponding unitary operation can be expressed as

$$R(\theta,\phi) = \mathrm{e}^{-\mathrm{i}Ht/\hbar} = \begin{pmatrix} \cos(\frac{\theta}{2}) & -\mathrm{i}\,\mathrm{e}^{-\mathrm{i}\phi}\sin(\frac{\theta}{2}) \\ -\mathrm{i}\,\mathrm{e}^{\mathrm{i}\phi}\sin(\frac{\theta}{2}) & \cos(\frac{\theta}{2}) \end{pmatrix}. \tag{3}$$

Here, $\theta = \Omega\tau$ represents the rotation angle, where τ is the pulse duration, while ϕ denotes the laser phase. Both parameters are precisely controllable through the duration and phase of the Raman beatnote that drives the qubit's Rabi oscillation. By optically addressing individual ions within a linear radio-frequency Paul trap, single-qubit rotations are implemented directly on targeted ions without introducing additional overhead.

Setting $\phi = 0$ produces a rotation about the x-axis by angle θ. The corresponding rotation operator is

$$R_X(\theta) = R(\theta,0) = \mathrm{e}^{-\mathrm{i}\frac{\theta}{2}\sigma_x} = \begin{bmatrix} \cos(\frac{\theta}{2}) & -\mathrm{i}\sin(\frac{\theta}{2}) \\ -\mathrm{i}\sin(\frac{\theta}{2}) & \cos(\frac{\theta}{2}) \end{bmatrix}. \tag{4}$$

Similarly, setting $\phi = \pi/2$ in the $R(\theta,\phi)$ gate yields a rotation about the y-axis by an angle θ, corresponding to

$$R_Y(\theta) = R(\theta,\frac{\pi}{2}) = \mathrm{e}^{-\mathrm{i}\frac{\theta}{2}\sigma_y} = \begin{bmatrix} \cos(\frac{\theta}{2}) & -\sin(\frac{\theta}{2}) \\ \sin(\frac{\theta}{2}) & \cos(\frac{\theta}{2}) \end{bmatrix}. \tag{5}$$

However, the implementation of the $R_Z(\theta)$ gate presents additional challenges. This gate operates on the phase of the quantum state, rather than inducing transitions between energy levels. Consequently, it cannot be directly realized with a single physical $R(\theta,\phi)$ pulse and typically requires a circuit composed of three $R(\theta,\phi)$ gates. It is given by

$$\begin{aligned} R_Z(\theta) &= \mathrm{e}^{-\mathrm{i}\frac{\theta}{2}\sigma_z} = \begin{bmatrix} \mathrm{e}^{-\mathrm{i}\frac{\theta}{2}} & 0 \\ 0 & \mathrm{e}^{\mathrm{i}\frac{\theta}{2}} \end{bmatrix} \\ &= R_Y\left(-\frac{\pi}{2}\right) R_X(\theta) R_Y\left(\frac{\pi}{2}\right). \end{aligned} \tag{6}$$

An alternative implementation involves using a single Stark shift pulse to directly modulate the qubit's energy levels. However, since this approach does not offer significantly higher fidelity compared to the standard $R(\theta,\phi)$ gate and does not notably simplify the circuit, there is limited practical incentive to pursue single-pulse realizations of the $R_Z(\theta)$ gate. Therefore, it is still common to use a combination of three $R(\theta,\phi)$ gates to implement the $R_Z(\theta)$ operation.

Trapped-ion systems inherently support scalable entangling gates. The MS gate[39] is implemented by using two off-resonant laser beams to simultaneously drive both the blue sideband and the red sideband transitions. During the system evolution, it generates a geometric phase that is independent of the initial state, thereby realizing controlled operations between ionic internal states. Because the MS gate is insensitive to motional states and does not require the ions to be cooled to the motional ground state, it can achieve high-fidelity entanglement through optimal physical parameters while exhibiting inherent robustness against certain experimental noise. The entangling MS gate can be expressed as

$$MS(\theta,\phi) = \mathrm{e}^{-\mathrm{i}\theta(S_x\cos(\phi)+S_y\sin(\phi))^2/4}. \tag{7}$$

Here, θ is the rotation angle, which corresponds to the strength of the two-body coupling. ϕ is the phase of the quantum gate, and $S_x = \sum_i \sigma_x^{(i)}$, $S_y = \sum_i \sigma_y^{(i)}$ are the total spin projections

along the x- and y-axes, respectively. For $\phi = 0$ or $\phi = \pi/2$, we obtain gates that act around the x- or y-axis, respectively, which correspond to Ising-XX and Ising-YY interactions. We denote them as

$$MS_{x,y}(\theta) = \mathrm{e}^{-\mathrm{i}\theta S_{x,y}^2/4}. \tag{8}$$

For the Ising-XX interaction, when the interaction involves only two qubits, the implemented quantum gate can be expressed as the unitary matrix

$$XX(\theta) = \begin{pmatrix} \cos(\frac{\theta}{2}) & 0 & 0 & -\mathrm{i}\sin(\frac{\theta}{2}) \\ 0 & \cos(\frac{\theta}{2}) & -\mathrm{i}\sin(\frac{\theta}{2}) & 0 \\ 0 & -\mathrm{i}\sin(\frac{\theta}{2}) & \cos(\frac{\theta}{2}) & 0 \\ -\mathrm{i}\sin(\frac{\theta}{2}) & 0 & 0 & \cos(\frac{\theta}{2}) \end{pmatrix}. \tag{9}$$

Experimentally, the Coulomb interaction facilitates coupling through shared phonon modes, which act as a bus for quantum information transfer. Throughout the laser pulse, the quantum state evolves conditionally on the motional mode, accumulating a geometric phase that leads to the desired entangling operation.

When a broad laser beam addresses the entire ion register, all ions can be simultaneously entangled, realizing a global $XX(\theta)$ gate described by the unitary operation

$$U_{GXX}(\theta) = \mathrm{e}^{-\mathrm{i}\frac{\theta}{2}\sum_{i<j}^{N}\sigma_x^i\sigma_x^j}, \tag{10}$$

where all pairwise couplings are simultaneously activated via laser-driven collective motional modes. It can be flexibly applied to any subset of qubits by selectively suppressing certain couplings.[41] In trapped-ion systems, through laser-driven sideband transitions, the system evolution operator can be written as

$$U_{GXX}(\tau) = \exp\left[\sum_{j,m}\beta_{j,m}(\tau)\sigma_x^j - \mathrm{i}\sum_{j<j'}\theta_{j,j'}\sigma_x^j\sigma_x^{j'}\right]. \tag{11}$$

Here, τ denotes the total operation time of the global entangling gate. σ_x^j is the Pauli X operator acting on the j-th qubit, and the index m labels the collective motional modes. $\beta_{j,m}(\tau) = \alpha_{j,m}(\tau)a_m^\dagger - \alpha_{j,m}^*(\tau)a_m$, where a_m ($a_m^\dagger$) is the annihilation (creation) operator of the m-th motional mode, and $\alpha_{j,m}(\tau)$ is the displacement of the j-th ion in the phase space of the m-th mode. $\theta_{j,j'}(\tau)$ denotes the effective coupling strength between the j-th and j'-th qubits. By independently modulating the laser phase and amplitude on each ion, both the closure of motional trajectories (which eliminates entanglement between the ions and the motional modes) and the uniform coupling strength among all ion pairs can be simultaneously achieved at the gate operation time τ.

This allows for the direct mapping of logical qubits onto physical qubits, eliminating the need for scheduling qubits via swap gates. Such flexibility significantly enhances the design of quantum circuits with diverse multi-qubit operations. In summary, to achieve efficient quantum circuit compilation on trapped-ion systems, the most promising strategy is to leverage the native gate set, comprising $R_X(\theta)$, $R_Y(\theta)$, $XX(\theta)$, and $GXX(\theta)$, as essential building blocks for VCOM, facilitating the efficient approximation of Pauli-string evolution operators $\mathrm{e}^{-\mathrm{i}Pt}$ in molecular Hamiltonian simulation.

2.2. Pauli string compilation for Hamiltonian simulation

A key application of quantum computing is the simulation of the time evolution of many-body quantum systems.[2] Such simulations not only enable the study of dynamical quantum behaviors,[42–45] but also serve as essential components in various quantum algorithms, including quantum phase estimation.[46,47] In the context of quantum simulation, the system Hamiltonian H_s must first be mapped to a qubit Hamiltonian H_q through math transformations such as the Jordan–Wigner (JW)[48] mapping or Bravyi–Kitaev (BK)[49] mapping.

The most widely used technique for implementing time evolution is the Trotter–Suzuki product formula,[50–53] along with its randomized variants.[54,55] The system Hamiltonian is expressed as $H_\mathrm{s} = \sum_{j=1}^{L}\alpha_j P_j$, where each P_j is a Pauli string and α_j is a real coefficient. The fundamental idea behind the Trotter–Suzuki product formula is to approximate the time evolution operator $\mathrm{e}^{-\mathrm{i}H_\mathrm{s}\delta t}$ using a sequence of operators from the set $\mathrm{e}^{-\mathrm{i}\alpha_j P_j\delta t}$. For instance, the first-order Trotter–Suzuki product formula provides the approximation

$$\mathrm{e}^{-\mathrm{i}H_\mathrm{s}\delta t} \approx \prod_{j=1}^{L}\mathrm{e}^{-\mathrm{i}\alpha_j P_j\delta t} + \mathcal{O}(\delta t^2). \tag{12}$$

Since the Trotter–Suzuki product formula generates an approximation of the time evolution operator that holds for arbitrary quantum states, the efficient compilation of Pauli strings into executable operations on quantum hardware becomes critical.

Whitfield *et al.*[53] introduced a quantum circuit implementation for the operator $\mathrm{e}^{-\mathrm{i}Pt}$, where P is a Pauli string of the form $P = P_1 \otimes P_2 \otimes \cdots \otimes P_n$, with each $P_j \in \{\sigma_x, \sigma_y, \sigma_z\}$. When the qubit operator is σ_x or σ_y, it can be transformed into σ_z through appropriate basis changes: $H\sigma_x H = \sigma_z$, and $S^\dagger H\sigma_y HS = \sigma_z$. Here, H is the Hadamard gate and S is the phase gate. Consequently, the unitary evolution operator $\mathrm{e}^{-\mathrm{i}Pt}$ can be expressed as

$$\begin{aligned} \mathrm{e}^{-\mathrm{i}Pt} &= \mathrm{e}^{-\mathrm{i}t\otimes_{j=1}^{n}P_j} \\ &= \mathrm{e}^{-\mathrm{i}t\otimes_{j=1}^{n}M_j^\dagger\sigma_z^{\otimes n}\otimes_{j=1}^{n}M_j} \\ &= \otimes_{j=1}^{n}M_j^\dagger\,\mathrm{e}^{-\mathrm{i}\sigma_z^{\otimes n}t}\otimes_{j=1}^{n}M_j. \end{aligned} \tag{13}$$

Here, the basis transformation M_j is defined according to the Pauli operator at the j^{th} position: it is chosen as the identity I if the operator is σ_z, as the Hadamard gate H if it is σ_x, or as $S^\dagger H$ if it is σ_y.

The core of this method lies in applying the global phase factor $e^{-i\delta t}$ arising from the unitary operator $e^{-iP_j\delta t}$ coherently across all qubits. Depending on the parity of the n-qubit computational basis state, if the parity is even, the phase shift applied is $e^{-i\delta t}$; if odd, it becomes $e^{i\delta t}$. This phase operation can be accurately implemented using an $R_Z(\theta)$ gate, which facilitates arbitrary phase shifts. The parity of the qubit register can be determined via a series of XOR operations. By performing bitwise XOR and evaluating the result, a final value of 0 corresponds to even parity, thus applying the phase $e^{-i\delta t}$, while a result of 1 indicates odd parity, leading to the phase $e^{i\delta t}$.

This is an example of a four-qubit connection achieved by applying multiple CNOT gates, as illustrated in Fig. 1. The role of the CNOT gates is to establish non-local correlations and enable phase information to propagate across qubits. Two circuit architectures can achieve this function. The first architecture is a chain structure, shown in Fig. 1(a), and it can be expressed as

$$\mathrm{CNOT_s} = \mathrm{CNOT}_{1\to2}\mathrm{CNOT}_{2\to3}\cdots\mathrm{CNOT}_{n-1\to n}. \quad (14)$$

M_j represents the basis transformation I, H or $S^\dagger H$ for the qubit operators σ_z, σ_x or σ_y, as shown in Eq. (13). Alternatively, the second architecture uses all qubits as controls targeting the same auxiliary qubit, as shown in Fig. 1(b), and it can be expressed as

$$\mathrm{CNOT_s} = \mathrm{CNOT}_{1\to n}\mathrm{CNOT}_{2\to n}\cdots\mathrm{CNOT}_{n-1\to n}, \quad (15)$$

which also facilitates phase propagation throughout the system.

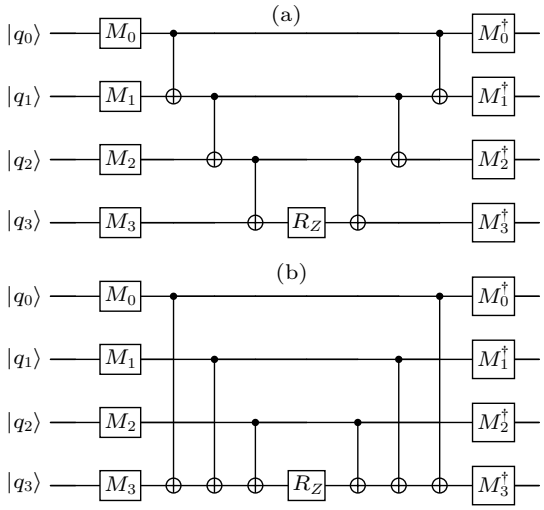


Fig. 1. We illustrate two methods for connecting multiple CNOT gates to qubits to realize an arbitrary Pauli string e^{-iPt}, using four qubits as an example. (a) A chain structure, where adjacent qubits are successively connected in sequence. (b) A configuration where all qubits act as controls, targeting the same auxiliary qubit. The global phase factor $e^{-i\delta t}$ is achieved through the $R_Z(\theta)$ gate. The single-qubit gate M_j corresponds to a basis transformation, with I, H, or $S^\dagger H$ applied to the qubit operators σ_z, σ_x, or σ_y, respectively.

However, high-level logical quantum gates must be decomposed into native gates that are compatible with the trapped-ion processors. These decompositions typically require the combination of multiple native gates to implement the functionality of a single logical gate,[28,29] which increases circuit depth and reduces the number of effective operations that can be performed within the available coherence time in the NISQ era.

2.3. Variational compilation optimization method for Pauli string implementation

Due to the limited coherence time inherent in current NISQ-era hardware, it is imperative to maximize the number of effective quantum gates within the constraints of shallow circuit depths. To address this critical challenge, we introduce a quantum compilation strategy specifically optimized for the native gate set of trapped-ion systems, employing a variational quantum algorithm framework. This method leverages the global entangling gate $GXX(\theta)$ to efficiently compile the time evolution operator of an arbitrary Pauli string, thus reducing circuit complexity. By significantly minimizing the circuit overhead while ensuring functional correctness, this strategy facilitates high-fidelity simulation of Hamiltonian dynamics, even under strict depth limitations.

A notable advantage of trapped-ion systems over other quantum platforms lies in their intrinsic long-range interactions, which enable the efficient implementation of global entangling gates. By utilizing the global entangling gate $GXX(\theta)$, the circuit depth can be substantially reduced. In this study, we adopt the native trapped-ion gates $R_X(\theta)$, $R_Y(\theta)$, and $GXX(\theta)$ as a universal gate set[56] for the construction of arbitrary Pauli strings. By employing suitable sequences of these gates, any unitary operation can be approximated with arbitrary precision.

We consider the evolution operator $e^{-i\alpha Pt}$ for a Pauli string P acting on an n-qubit system. This operation can be implemented using a sequence of m native gates, as follows:

$$\begin{aligned}|\mathrm{out}\rangle &= e^{-i\alpha Pt}|\mathrm{in}\rangle \\ &= G_m(\theta_m)G_{m-1}(\theta_{m-1})\cdots G_1(\theta_1)|\mathrm{in}\rangle. \end{aligned} \quad (16)$$

While the input and output states uniquely determine the evolution matrix, the number and structure of the gates required to realize this transformation are not unique. Our objective is to identify the shallowest possible quantum circuit that implements this evolution using only native trapped-ion gates.

To achieve this, we leverage the Hermitian conjugate of the evolution operator, $e^{i\alpha Pt}$, which corresponds to the inverse of the original circuit. Applying both operators sequentially gives

$$\begin{aligned}|\mathrm{out}\rangle &= \left(G_1^{-1}(\theta_1)G_2^{-1}(\theta_2)\cdots G_m^{-1}(\theta_m)\right) \\ &\quad \left(G_m(\theta_m)G_{m-1}(\theta_{m-1})\cdots G_1(\theta_1)\right)|\mathrm{in}\rangle\end{aligned}$$

$$= e^{i\alpha Pt} e^{-i\alpha Pt} |\text{in}\rangle$$
$$= I|\text{in}\rangle. \quad (17)$$

This ensures that the initial state is preserved, which is equivalent to implementing the identity unitary transformation. By verifying whether the final state equals the initial state, i.e., $|\text{out}\rangle = |\text{in}\rangle$, one can determine whether the desired target quantum circuit has been realized. The Hermitian conjugate of the evolution operator, $e^{i\alpha Pt}$, is straightforward to construct and can be realized using standard quantum circuit decomposition techniques. As illustrated in Fig. 1, this can be implemented by adjusting the angle of the $R_Z(\theta)$ gate within the CNOT-based structure to a negative value. Denote the circuit for $e^{i\alpha Pt}$ as $S_k S_{k-1} \cdots S_1$. The objective is to optimize the quantum circuit such that the output state remains identical to the input state

$$|\text{out}\rangle = (S_k S_{k-1} \cdots S_1) (G_m(\theta_m) G_{m-1}(\theta_{m-1}) \cdots G_1(\theta_1)) |\text{in}\rangle. \quad (18)$$

In this framework, our hardware-efficient ansatz varies depending on the input Pauli strings, and not every layer is exactly the same. When the input string acts on a single qubit, we sequentially apply the quantum gates $R_Y(\theta_1)$, $R_X(\theta_2)$, and $R_Y(\theta_3)$ to the corresponding qubit, without requiring any other operations, because such a sequence of three gates can implement an arbitrary single-qubit unitary operation. By adjusting the three parameters, it can cover the entire two-dimensional Hilbert space, thereby realizing an arbitrary unitary rotation. When the input string acts on multiple qubits, we alternately apply single-qubit gates and global $GXX(\theta)$ gates; in this case, the global $GXX(\theta)$ gates provide entanglement capability for the circuit. In the circuit, we alternately implement rotation gates around the x-axis and the y-axis because they do not commute. Using such an ansatz allows us to cover the entire Hilbert space without introducing too much redundancy. Figure 2 shows an example ansatz acting on four qubits. The number of layers in the hardware-efficient ansatz directly corresponds to the number of Pauli strings in the input Hamiltonian. The circuit architecture is fixed, meaning the positions of all gates remain unchanged, while their parameters are optimized.

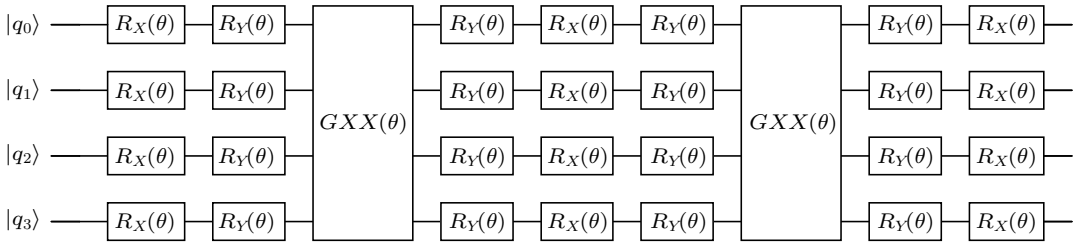


Fig. 2. When the input string acts on multiple qubits, the variational optimization circuit uses the ansatz, which is an example of a 4-qubit. It is achieved by alternately acting single-qubit gates and global entanglement gates.

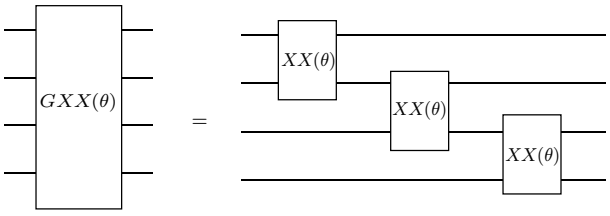


Fig. 3. When constructing a hardware-efficient ansatz using only two-qubit $XX(\theta)$ gates, taking four qubits as an example, sequentially connected $XX(\theta)$ gates are used to replace a single global $GXX(\theta)$ gate, thereby providing entanglement capability for the circuit.

A Pauli string composed of N qubits requires $7N$ single-qubit gates and 2 global $GXX(\theta)$ gates. For M strings, only $2M$ global $GXX(\theta)$ gates are required to realize the quantum circuit, and at most $7NM$ single-qubit gates are needed. If we do not use the global $GXX(\theta)$ gates for optimization here, but only use $XX(\theta)$ gates, and cascade them to replace the positions of the global $GXX(\theta)$ gates, then the number of $XX(\theta)$ gates required is $2M(N-1)$. The specific method of replacing the global $GXX(\theta)$ gates with $XX(\theta)$ gates is illustrated in Fig. 3, where the $XX(\theta)$ gates are connected in sequence to provide entanglement capability for the circuit. When targeting a specific Hamiltonian, the number of circuit layers and quantum gates required for the entire circuit will be far less than the above maximum values. After different mathematical mappings, the number of Pauli strings involved in the qubit Hamiltonian varies, and the number of qubits in each string also differs. However, in practical optimization, employing a smarter mathematical mapping can further reduce the number of optimization parameters in the quantum circuit.

To enhance optimization performance, we adopt a hybrid strategy that combines genetic algorithms and gradient descent. The cost function $C(\theta_i)$ is defined as

$$C(\theta_i) = \sum_s (1 - |\langle \psi_{\text{out}} | \rho_{\text{in}} | \psi_{\text{out}} \rangle|_s^2), \quad (19)$$

where $|\psi_{\text{out}}\rangle$ represents the output state and ρ_{in} denotes the input density matrix. This cost function quantifies the deviation between the final and initial states across all training sequences, thereby guiding the parameter search towards higher-fidelity implementations until $|\text{out}\rangle = |\text{in}\rangle$. Since the initial state is randomly selected, it is possible for the chosen input state to be too specific, thereby limiting the generalization to other quantum states. To improve the generalization capability of the optimized circuit, we simultaneously train over seven

randomly chosen initial states, thereby reducing the reliance on an arbitrary particular input state. The number of training initial states chosen here depends on the specific situation. As the number of qubits in the circuit increases, the involved Hilbert space grows, and we need to correspondingly increase the number of training initial states.

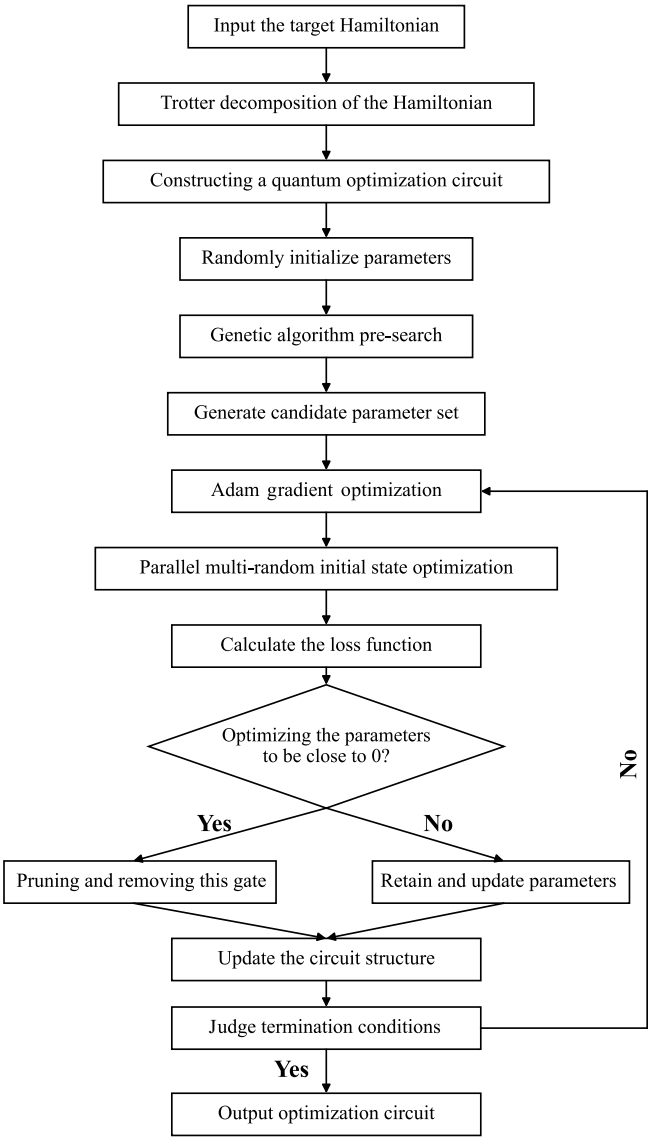


Fig. 4. Workflow of the variational compilation optimization method for implementing the target Hamiltonian's evolution operator.

Direct gradient optimization from random parameter initialization may lead to unstable convergence and an increased tendency to converge to local optima, thus impeding the achievement of a globally optimal or high-performance solution. To address these challenges, we first employ a genetic algorithm for pre-optimization. The parameter initialization range is set to $[-\pi/4, \pi/4]$, and the initial parameters are randomly generated based on a uniform distribution. The population consists of 30 individuals, and the algorithm is iterated for 50 generations using a strategy that incorporates single-point crossover and random mutation. This global search method efficiently explores a broad parameter space, allowing for the identification of promising initial points for subsequent local refinement. This hybrid approach significantly increases the likelihood of discovering high-quality solutions and enhances the stability and reproducibility of the optimization process.

For the gradient-based optimization phase, we employ the adaptive moment estimation (ADAM)[57] optimizer, known for its effectiveness in managing non-convex optimization landscapes and its robust performance in high-dimensional parameter spaces. In this stage, the optimal solution obtained from the genetic algorithm is used as the initial parameter for further optimization, with a learning rate set to 0.01. During training, we also prune the circuit by deactivating quantum gates with negligibly small parameters. Since these gates contribute minimally to the loss function, essentially behaving as identity operations with vanishing gradients, their removal has a negligible impact on overall performance, while simplifying the circuit structure. A schematic outlining the VCOM workflow for implementing the target Hamiltonian's evolution operator is shown in Fig. 4.

We applied the proposed VCOM method to simulate the evolution of molecular Hamiltonians, demonstrating its performance on hydrogen chains of varying lengths. Hydrogen chains are widely used as test molecules because they strike an ideal balance between simplicity and complexity. Their electronic structure is simple: for N atoms, there are $2N$ spin orbitals, requiring only $2N$ qubits for simulation. This stands in stark contrast to molecules like nitrogen chains or water, which often demand 10–20 qubits or more, accompanied by deep circuits. Moreover, hydrogen chains are among the few systems for which the exact ground-state energy (within chemical accuracy) can be obtained on classical computers using density matrix renormalization group. The Hamiltonian of the hydrogen chain in the second quantization can be expressed as

$$H = \sum_{pq} h_{pq} a_p^\dagger a_q + \frac{1}{2} \sum_{pqrs} h_{pqrs} a_p^\dagger a_q^\dagger a_r a_s, \tag{20}$$

in which the wave function's antisymmetry is enforced through the anticommutation relations of the fermion creation and annihilation operators $a_i^\dagger$ and a_j. Encoding the electron's spatial and spin coordinates as $\sigma_i = (r_i, s_i)$, the two sets of scalar coefficients can be calculated via

$$\begin{aligned} h_{pq} &= \int \mathrm{d}\sigma \phi_p^*(\sigma) \left(\frac{\nabla_r^2}{2} - \sum_i \frac{Z_i}{|R_i - r|} \right) \phi_q^*(\sigma), \\ h_{pqrs} &= \int \mathrm{d}\sigma_1 \mathrm{d}\sigma_2 \frac{\phi_p^*(\sigma_1)\phi_q^*(\sigma_2)\phi_s(\sigma_1)\phi_r(\sigma_2)}{|r_1 - r_2|}. \end{aligned} \tag{21}$$

Here, in atomic units ($\hbar = 1$), R_i, Z_i are the positions and charges of the nuclei, and r_i are the positions of the electrons. In order to implement the Hamiltonian on a qubit-based

quantum simulator, fermionic Hamiltonians need to be transformed to spin Hamiltonians. The Jordan–Wigner transformation serves as a key bridge connecting fermionic systems with qubit systems. It can precisely map fermionic creation and annihilation operators to Pauli operators on qubits, thereby making it possible to simulate fermionic systems on quantum computers. Specifically, it stores the occupation number information locally on individual qubits, while encoding the phase information (the anticommutation relations) through a nonlocal string operator (a string of σ_z).

Initially, we simulated the H_2 molecule at its equilibrium geometry, with a distance of 0.7414 Å between the two hydrogen atoms. In the STO-3G basis set, the H_2 Hamiltonian can be expressed as 4 qubits and 15 Pauli strings in an active space by JW transformation. That is

$$\begin{aligned} H_{\mathrm{H}_2} = {} & c_0 I + c_1 Z_0 + c_2 Z_1 + c_3 Z_2 + c_4 Z_3 + c_5 Z_0 Z_1 + c_6 Z_0 Z_2 \\ & + c_7 Z_0 Z_3 + c_8 Z_1 Z_2 + c_9 Z_1 Z_3 + c_{10} Z_2 Z_3 + c_{11} X_0 X_1 Y_2 Y_3 \\ & + c_{12} X_0 Y_1 Y_2 X_3 + c_{13} Y_0 X_1 X_2 Y_3 + c_{14} Y_0 Y_1 X_2 X_3, \end{aligned} \tag{22}$$

where the coefficients c_i depend on the internuclear separation R between the hydrogen atoms and are derived from the integrals h_{pq} and h_{pqrs}; their specific values are provided in Appendix A. Beginning from the Hartree–Fock state $|1100\rangle$, we simulated the time evolution up to $T = 4$ using both first- and second-order Trotter–Suzuki product formulas with a time step of $\delta t = 0.04$. This determines the scale of the circuit ultimately used for optimization. This part can be represented as a workflow in Fig. 5. The numbers and fidelities of quantum gates required by different methods are summarized in Table 1. For the first- and second-order Trotter–Suzuki product formulas, methods based on standard quantum circuit decomposition (SQCDM) require the following gate counts: the first-order approach uses 6200 single-qubit gates and 3600 CNOT gates, while the second-order approach requires 12400 single-qubit gates and 7200 CNOT gates.

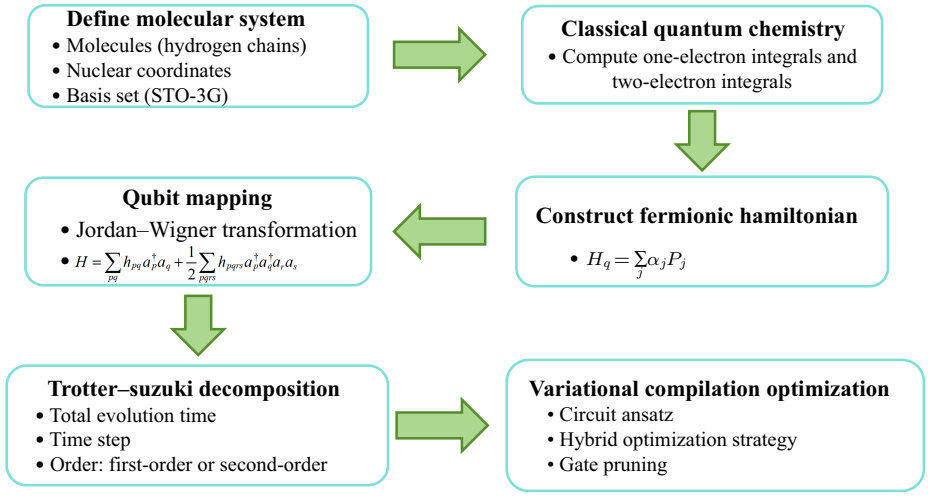


Fig. 5. Workflow from molecular specification to assembled optimized circuits. The process begins with defining the molecular system (H_2, H_3, H_4) and computing one- and two-electron integrals via classical quantum chemistry calculations. The fermionic Hamiltonian is then mapped to a Pauli Hamiltonian using the Jordan–Wigner transformation. After Trotter–Suzuki product formulas, each Pauli string evolution is compiled into a shallow native-gate circuit using VCOM. Finally, these compiled circuits are assembled in both first- and second-order Trotter–Suzuki product formulas to form the complete time-evolution circuit. This workflow directly addresses the core steps from molecular selection to circuit assembly.

Table 1. Performance comparison of H_2 Hamiltonian simulation methods: gate counts and fidelities at $\delta t = 0.04$, $T = 4$. We compare the performance of three methods under both first- and second-order Trotter–Suzuki product formulas: the standard quantum circuit decomposition method (SQCDM), the native gate decomposition method (NGDM), and the variational compilation optimization method (VCOM) using $GXX(\theta)$ and $XX(\theta)$ gates. In the simulation, we assume perfect quantum gates and that no noise is introduced throughout the simulation process.

Trotter	SQCDM		NGDM		VCOM ($GXX(\theta)$)			VCOM ($XX(\theta)$)		
	Single	CNOT	Single	$XX(\theta)$	Single	$GXX(\theta)$	Fidelity	Single	$XX(\theta)$	Fidelity
1st-order	6200	3600	37000	3600	8800	600	99.659%	10100	600	99.715%
2nd-order	12400	7200	74000	7200	14400	700	99.585%	15400	900	99.716%

When decomposed further into the native trapped-ion gate set using the native gate decomposition method (NGDM), the circuit depth increases significantly, requiring 37000 single-qubit gates and 3600 $XX(\theta)$ gates for the first-order Trotter–Suzuki product formula method. For the second-order Trotter–Suzuki product formula, the quantum circuit depth increases even further, with 74000 single-qubit native gates and 7200 two-qubit $XX(\theta)$ gates. Although the number of two-qubit gates remains constant, the count of single-qubit gates increases nearly sixfold, substantially deepening the circuit, which in turn introduces more noise and compromises the reliability of the results. In contrast, VCOM, which utilizes the

native $GXX(\theta)$ gate, significantly reduces the number of entangling and single-qubit operations. In the first-order Trotter–Suzuki product formula, only 600 native $GXX(\theta)$ gates and 8800 single-qubit native gates are needed, achieving a fidelity of 99.659%. For the second-order Trotter–Suzuki product formula, the method requires only 700 native $GXX(\theta)$ gates and 14400 single-qubit native gates, yielding a fidelity of 99.585%. Due to the large number of quantum gates involved, the introduction of noise can cause significant distortion and reduce the reliability of the results. However, since all the quantum gates used in this study are assumed to be perfect and noise-free, the fidelity in both the SQCDM and NGDM schemes is equal to 1.

We also compare the total gate consumption and the ratio of multi-qubit gates in the NGDM and VCOM methods, as shown in Fig. 6. In the VCOM method, not only is the total number of gates significantly reduced, but the proportion of multi-qubit gates is also lower. Specifically, in the first- and second-order Trotter–Suzuki product formula methods, only 6.4% and 4.6% of the gates, respectively, are multi-qubit gates. In contrast, the NGDM method requires 8.9% multi-qubit gates in both the first- and second-order approaches. The reduction in gate operations mitigates the impact of hardware noise, thereby enabling more effective operations within the same coherence window and enhancing computational efficiency. Our native gate compilation strategy demonstrates substantial potential for efficiently utilizing NISQ-era hardware capabilities.

Although the global entangling $GXX(\theta)$ gate significantly reduces circuit depth, two-qubit entangling $XX(\theta)$ gates remain more practical in the NISQ era due to their higher technological maturity, greater operational accuracy, and reduced crosstalk. These gates can be reliably implemented using precisely controlled laser pulses. In this work, we also explore an alternative gate set consisting solely of native single-qubit gates $R_X(\theta)$ and $R_Y(\theta)$, combined with the two-qubit $XX(\theta)$ gate, all of which are directly available in trapped-ion processors. This gate set is employed to natively construct quantum circuits for arbitrary Pauli strings, offering a hardware-efficient compilation approach optimized for current device capabilities.

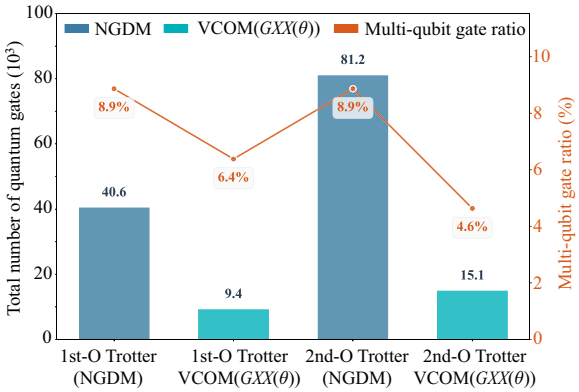


Fig. 6. Comparison of total gate counts and multi-qubit gate proportions for H_2 Hamiltonian simulations using first- and second-order Trotter–Suzuki product formulas, with the native gate decomposition method (NGDM) and the variational compilation optimization method (VCOM).

We also simulated the time evolution of the H_3 and H_4 molecular Hamiltonians under identical conditions in the STO-3G basis set using both first- and second-order Trotter–Suzuki product formulas. The specific configurations and Hamiltonian representations of the two molecules are presented in Appendix A. The H_3 Hamiltonian is mapped onto 6 qubits through the application of 62 Pauli strings via the Jordan–Wigner transformation, and the Hartree–Fock state can be represented as $|111000\rangle$. The H_4 Hamiltonian is mapped onto 8 qubits, comprising 93 Pauli strings via the same transformation, with the initial state set to $|11110000\rangle$. The time evolution was simulated up to $T = 4$ with a time step of $\delta t = 0.04$. The quantum gates required and the corresponding fidelities for the three methods (SQCDM, NGDM, and VCOM) are presented in Tables 2 and 3.

Table 2. Performance comparison of H_3 Hamiltonian simulation methods: gate counts and fidelities at $\delta t = 0.04$, $T = 4$. We compare the performance of three methods under both first- and second-order Trotter–Suzuki product formulas: the standard quantum circuit decomposition method (SQCDM), the native gate decomposition method (NGDM), and the variational compilation optimization method (VCOM) using $GXX(\theta)$ and $XX(\theta)$ gates. In the simulation, we assume perfect quantum gates and that no noise is introduced throughout the simulation process.

Trottor	SQCDM		NGDM		VCOM ($GXX(\theta)$)			VCOM ($XX(\theta)$)		
	Single	CNOT	Single	$XX(\theta)$	Single	$GXX(\theta)$	Fidelity	Single	$XX(\theta)$	Fidelity
1st-order	42100	31000	288300	31000	59900	1900	99.180%	62100	3100	98.181%
2nd-order	84200	62000	576600	62000	100300	2900	96.339%	132000	6100	98.393%

Table 3. Performance comparison of H_4 Hamiltonian simulation methods: gate counts and fidelities at $\delta t = 0.04$, $T = 4$. We compare the performance of three methods under both first- and second-order Trotter–Suzuki product formulas: the standard quantum circuit decomposition method (SQCDM), the native gate decomposition method (NGDM), and the variational compilation optimization method (VCOM) using $GXX(\theta)$ and $XX(\theta)$ gates. In the simulation, we assume perfect quantum gates and that no noise is introduced throughout the simulation process.

Trottor	SQCDM		NGDM		VCOM ($GXX(\theta)$)			VCOM ($XX(\theta)$)		
	Single	CNOT	Single	$XX(\theta)$	Single	$GXX(\theta)$	Fidelity	Single	$XX(\theta)$	Fidelity
1st-order	76400	52000	496400	52000	86200	1500	99.061%	122300	6800	97.966%
2nd-order	152800	104000	992800	104000	179100	3500	97.918%	228500	11400	96.215%

For the H_3 molecule, when using the SQCDM method for the first-order Trotter–Suzuki product formula, the circuit requires 42100 single-qubit gates and 31000 CNOT gates. Decomposing this into the native gate set using the NGDM method leads to a significant increase in gate counts, with 288300 single-qubit gates and 31000 multi-qubit $XX(\theta)$ gates. For the second-order Trotter–Suzuki product formula, both the number of single-qubit gates and multi-qubit gates must be doubled. In contrast, our method requires only 59900 single-qubit gates and 1900 multi-qubit $GXX(\theta)$ gates in the first-order Trotter–Suzuki product formula, achieving a fidelity of 99.180%. For the second-order Trotter–Suzuki product formula, only 2900 multi-qubit $GXX(\theta)$ gates are needed, with a fidelity of 96.339%.

For the H_4 molecule, in the first-order Trotter–Suzuki product formula, the SQCDM method requires 76400 single-qubit gates and 52000 CNOT gates. When decomposing to the native gate set using the NGDM method, the gate counts increase significantly, requiring 496400 single-qubit gates and 52000 two-qubit $XX(\theta)$ gates. In contrast, the VCOM method only requires 86200 single-qubit gates and 1500 $GXX(\theta)$ gates, achieving a fidelity of 99.061%. For the second-order Trotter–Suzuki product formula, the number of required single-qubit and multi-qubit gates doubles in both the SQCDM and NGDM methods. However, in the VCOM method, only 179100 single-qubit gates and 3500 $GXX(\theta)$ gates are needed, with a fidelity of 97.918%.

We compared the time evolution of the H_2, H_3, and H_4 molecular Hamiltonians under identical conditions using second-order Trotter–Suzuki product formulas. The two schemes based on the VCOM method employed either global $GXX(\theta)$ gates or two-qubit $XX(\theta)$ gates, as shown in Fig. 7. It is evident that the proportion of two-qubit gates in the scheme utilizing global $GXX(\theta)$ gates is lower than that in the scheme using two-qubit $XX(\theta)$ gates. In the simulations of the three molecules, 4.6%, 2.8%, and 1.9% of the gates are multi-qubit gates in the $GXX(\theta)$ scheme, while the $XX(\theta)$ scheme requires 5.5%, 4.4%, and 4.8%, respectively. Furthermore, as circuit complexity increases with system size, the number of required two-qubit $XX(\theta)$ gates also rises. Nonetheless, this approach still offers significant advantages over the NGDM scheme.

The proposed VCOM framework presents a significant leap forward in optimizing Pauli string implementations for trapped-ion systems. By leveraging the native gate set, including $R_X(\theta)$, $R_Y(\theta)$, and global $GXX(\theta)$ gates, our approach minimizes circuit depth while enhancing computational efficiency. Through a hybrid optimization strategy combining genetic algorithms and gradient descent, our method ensures high-fidelity simulation of molecular Hamiltonians within the stringent constraints imposed by current NISQ-era hardware. Crucially, this approach reduces the reliance on multi-qubit gates and the overall circuit depth, making it highly suitable for practical quantum simulations. This work lays the foundation for future advancements in quantum compilation, enabling more efficient simulations on trapped-ion platforms.

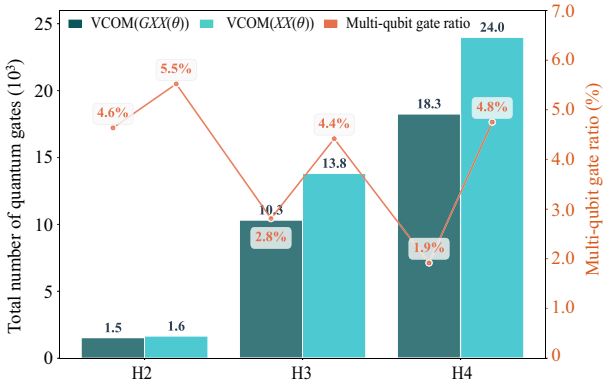


Fig. 7. We compare the total number of quantum gates and the corresponding ratios of entanglement gates required in the variational compilation optimization method (VCOM) schemes, which utilize global $GXX(\theta)$ and two-qubit $XX(\theta)$ gates, respectively, in the second-order Trotter–Suzuki product formula for the simulations of the H_2, H_3, and H_4 molecules.

3. Discussion

In this work, we present a VCOM method specifically designed for trapped-ion systems. By utilizing native gates, specifically single-qubit rotations ($R_X(\theta)$, $R_Y(\theta)$) and entangling gates ($XX(\theta)$ and $GXX(\theta)$), our approach enables efficient simulation of molecular Hamiltonians with optimized resource usage. We integrate a hybrid optimization technique, combining a genetic algorithm with gradient-based optimization, and incorporate dynamic gate pruning to reduce circuit depth. This approach significantly decreases both the circuit depth and the proportion of multi-qubit gates, thereby improving resource efficiency on current NISQ-era hardware.

Theoretically, a global entangling gate can directly entangle multiple ions, eliminating the need to sequentially apply a series of two-qubit entangling gates to achieve the same effect. However, in practical experiments, factors such as the coherence time of trapped ions, the fidelity of individual entangling gates, and the operation duration must also be considered.

Two-qubit entangling gates typically rely on driving a single collective motional mode to generate entanglement, but this approach encounters challenges such as mode crosstalk and isolation difficulties as the number of ions increases, leading to slower gate speeds and reduced fidelity. By precisely modulating the laser field and implementing multi-mode coupling, the approach demonstrated by Lu *et al.*[41] enables independent control of each ion. By adjusting the phase and amplitude of the pulses, a uniform coupling strength can be achieved, enabling the implementation of a global entangling gate for an arbitrary number of ions. This method is more

scalable compared to single-mode approaches. It takes 80 microseconds to entangle three qubits and 120 microseconds to entangle four qubits. As the number of participating particles increases, the time required to implement the gate grows linearly, with a time complexity of $O(N)$.

Currently, implementing a two-qubit entangling gate typically requires tens to hundreds of microseconds. The higher the required fidelity, the longer the duration needed. For example, the Helios quantum computer[58] demonstrates a high-fidelity entangling gate operation with 99.92% accuracy, completed within approximately 70 microseconds. Using sequential two-qubit gates, generating 4-qubit entanglement takes at least 280 microseconds, whereas using a global entangling gate requires only 120 microseconds. This significantly increases the number of quantum operations that can be performed within the coherence time. As the number of qubits required to achieve quantum entanglement increases, the advantages of using global entangling gates become more significant — particularly when simulating complex Hamiltonians.

Although the fidelity of the global entangling gate achieved by current methods has not yet matched the highest fidelity of two-qubit entangling gates, further reductions in factors such as laser beam fluctuations, mode frequency offsets, and crosstalk could improve fidelity. In complex molecular simulations, noise accumulation arises from both gate operations and system decoherence. Employing a global entangling gate can substantially reduce the time needed for simulation operations and thereby enhance the reliability of the results.

In the current NISQ era, quantum hardware is confronted not only with limited coherence times but also with imperfections in quantum gates arising from inherent noise. To realize practical quantum applications, it is essential to account for these noise effects throughout the computational process. In trapped-ion systems, interactions between qubits and their environment can introduce noise during quantum operations. In this study, we evaluate the performance under realistic noise conditions, including laser intensity noise and phase noise. Simulations confirm that our method maintains high fidelity under such noise, demonstrating strong resilience and suitability for implementation in the NISQ era.

When ions are sufficiently confined and cooled, the dominant source of error originates from imperfections in the laser system. Lasers play a central role in trapped-ion quantum computing, functioning as the universal control interface for initialization, quantum operations, and readout. Precise laser control is therefore indispensable, as quantum information processing in such systems would otherwise be infeasible. Although arbitrary single-qubit rotations can be realized by tuning the duration (which determines the rotation angle θ), phase (which sets the rotation axis in the XY plane), and intensity of the laser pulses, practical limitations in laser stability introduce noise. These fluctuations reduce gate fidelity and compromise the reliability of computational outcomes.

We simultaneously consider both laser intensity noise and phase noise. Even with state-of-the-art feedback control systems, laser intensity cannot be perfectly stabilized and remains subject to small, rapid fluctuations. Such fluctuations directly induce errors in the rotation angles of quantum gates. An ideal single-qubit gate, such as $R(\theta)$, is realized by applying a resonant laser pulse, where the rotation angle θ is given by the product of the Rabi frequency Ω and the pulse duration τ. In practice, however, intensity noise leads to deviations from the intended operation, yielding $R(\theta+\delta)$, where δ represents a small random angular error drawn from a Gaussian distribution. This deviation causes discrepancies between the actual and target quantum states. The effect of intensity noise is generally more pronounced in multi-qubit gates than in single-qubit gates, owing to their greater complexity, longer operation times, and heightened sensitivity to parameter fluctuations. For simplicity, we model this effect by introducing a random angular deviation δ to the rotation angle in multi-qubit operations as well.

Laser phase noise represents another critical source of decoherence, characterized by stochastic and unpredictable fluctuations in the phase of the laser that drives quantum gate operations. This noise is intrinsic to the laser, as no practical source can generate perfectly monochromatic and phase-stable light. Multiple factors, including temperature variations, mechanical vibrations within the laser cavity, and the fundamental quantum properties of the lasing medium, contribute to these random phase shifts. The execution of high-fidelity quantum gates relies on precisely controlled laser pulses to drive specific quantum transitions, and the accuracy of this process is highly sensitive to the phase stability of the laser throughout the pulse duration. Phase fluctuations during a pulse cause the effective rotation axis of the qubit to vary randomly, which is equivalent to superimposing an unknown Z-rotation error on the ideal gate operation.

To simulate the cumulative effect of phase noise, we adopt a simplified model by applying a static random phase error to each gate operation. Specifically, for every gate, a random phase offset δ is sampled from a Gaussian distribution and incorporated into the gate dynamics. For example, an ideal gate operation $U_{\text{ideal}} = R(\theta)$ subject to phase noise is modeled as

$$U_{\text{actual}} = R_Z(\delta)\cdot R(\theta)\cdot R_Z(-\delta). \tag{23}$$

For multi-qubit gates, the same model is applied for simplicity, with a phase error $R_Z(\delta)$ introduced independently on each participating qubit.

To demonstrate the enhanced noise resilience of our approach, we evaluated the fidelity of random Hamiltonian compilations at various scales under noisy conditions, as illustrated in Fig. 8. For each computational task involving a specific number of qubits, we constructed a set of random test Hamiltonians. Each Hamiltonian H is composed of a linear combination of three random Pauli strings and can be represented as

$$H = \sum_{k=1}^{3} c_k \otimes_{i=1}^{n} P_i^{(k)}. \tag{24}$$

Here, n is the number of qubits, k labels the different Pauli string items (three items in total), c_k is the k^{th} randomly generated real coefficient, and $P_i^{(k)} \in X, Y, Z$ is the Pauli operator acting on the i^{th} qubit. Both the NGDM and VCOM circuit compilation strategies are compared under identical noise levels. Direct decomposition into the native gate set using the NGDM method not only significantly increases circuit depth but also amplifies noise effects, leading to a marked reduction in fidelity. This degradation becomes progressively more severe as the number of qubits increases, eventually causing the results to be overwhelmed by noise. In contrast, our compilation strategy achieves both shallow circuit depth and strong noise tolerance. When only two-qubit $XX(\theta)$ gates are used in the optimization scheme, the improvement becomes more pronounced as circuit complexity increases. Furthermore, if the native $GXX(\theta)$ gate is employed, the performance is enhanced even further. The fidelity remains stable and does not deteriorate rapidly with increasing circuit complexity, indicating that larger-scale circuits can be optimized without sacrificing accuracy.

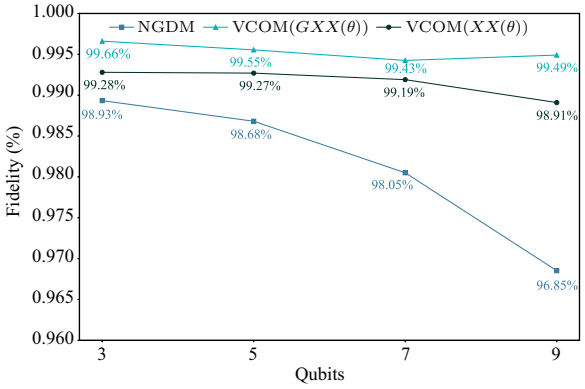


Fig. 8. Comparative noise resilience under laser intensity and phase noise. Simulated fidelity of time-evolution circuits compiled using NGDM and VCOM (with both $GXX(\theta)$ and $XX(\theta)$ entangling gates) for random Hamiltonians with increasing number of qubits n.

In this scheme, we assume that the complete hardware-efficient circuit can be directly obtained from the target Hamiltonian. When the target Hamiltonian is small in scale, the number of parameters to be optimized is relatively small, allowing the optimization to be performed effectively and achieving optimal results. However, as the system scale grows, the number of variational parameters requiring optimization increases, thereby raising the complexity of the optimization process.

The optimization complexity of the entire hardware-efficient circuit is positively correlated with both the number of distinct Pauli strings and the optimization cost per string. For a hardware-efficient ansatz, as the problem scale expands, the gradient of the loss function diminishes exponentially and approaches zero, resulting in barren plateaus. Since in this scheme the number of parameters increases linearly with the number of qubits in the Hamiltonian, and the hybrid optimization strategy combining a genetic algorithm and gradient descent exhibits good global search capability, it is expected that optimization remains controllable within the range of 10 to 20 qubits.

When the number of qubits is limited but the circuit depth is substantial, a trade-off can be made between optimization accuracy and circuit depth. Through blockwise optimization, we reduce the number of parameters optimized simultaneously at each step. Specifically, by truncating the qubit Hamiltonian into an appropriate number of parts, the optimization parameters associated with the Pauli strings in each part can be tuned to find the optimal solution. Although this method increases the depth of the final circuit to some extent, it remains significantly more efficient than direct decomposition. Consequently, optimization can be achieved even for larger-scale Hamiltonians.

In addition, since a global entangling gate is used here, fewer quantum gates are required compared to using two-qubit entangling gates to establish connections between qubits. This results in a reduction in the number of optimization parameters. As the system scale increases, the number of parameters that need to be optimized grows more slowly. The more qubits involved in a string, the more pronounced the advantages of using a global entangling gate become. Compared to directly using the hardware-efficient ansatz, this approach offers greater benefits when addressing problems of the same scale, as it requires fewer parameters to be optimized and results in a shallower quantum circuit.

In the NISQ era, one of the most critical challenges is to reduce quantum circuit depth, ensuring that computation completes within the system's coherence time. Various compilation techniques have been developed to optimize existing circuits, such as Clifford-grouping-based methods,[22,23] which compress Trotterized Pauli exponentials into shallower circuits. Separately, the Hamiltonian variational ansatz (HVA)[20,21] offers a physically motivated circuit construction that naturally yields shallow depth for certain Hamiltonians, without requiring the compression of an existing circuit. Both approaches help improve the reliability of results on NISQ devices.

Clifford grouping methods are primarily designed to reduce the measurement overhead in VQE by partitioning Pauli strings into commuting sets that can be simultaneously diagonalized via Clifford circuits.[22,23] They are not only highly effective for ground-state energy estimation but also applicable to time-evolution simulations, where multiple commuting Pauli exponentials can be combined into a single unitary, thereby reducing the number of Trotter steps and the overall circuit depth. However, this approach requires substantial classical preprocessing to identify optimal commuting sets and construct the corresponding Clifford circuits. Moreover, its efficiency is highly sensitive to the commutativity structure of the Hamiltonian, which becomes nontrivial for large molecular systems. In contrast, VCOM adopts a complementary strategy. Instead of merging multiple Pauli strings, it directly compiles each individual Pauli string evolution operator $e^{-i\theta P}$ using the native gate set of trapped-ion processors.

The HVA constructs variational circuits by alternating evolution under the constituent terms of the Hamiltonian. This approach is particularly powerful for models with a small number of terms and inherent symmetries, such as the Hubbard model, where the circuit structure naturally aligns with the Hamiltonian. However, for molecular Hamiltonians in quantum chemistry, which often contain hundreds of Pauli strings with complex coefficients, HVA leads to deep circuits and a large number of variational parameters, exacerbating the barren plateau problem. VCOM, in contrast, maintains a fixed and shallow circuit architecture for each Pauli string, with a parameter count that scales linearly with the number of qubits and layers. This makes VCOM well-suited for molecular systems where the Hamiltonian contains many terms, whereas HVA excels when the Hamiltonian is compact and symmetric. In summary, VCOM occupies a distinct niche in the landscape of quantum compilation: it is a hardware-native, structure-agnostic method optimized for compiling Pauli string evolution operators in time-evolution simulations on trapped-ion platforms. It does not conflict with existing Pauli-string-based compilation schemes for circuit compression; the logical circuit obtained after optimization can still be further optimized using such schemes. It provides an efficient, hardware-tailored route for implementing individual Pauli exponentials within Trotter-based dynamics on near-term hardware.

4. Conclusion

In summary, we have proposed VCOM, a method that directly utilizes the native gates available in trapped-ion systems to compile Pauli strings and apply them to the simulation of small-molecule Hamiltonians. By combining genetic algorithm pre-training with ADAM gradient descent and dynamically pruning redundant gates, our method achieves high fidelity while compressing the original quantum circuit. The proposed approach offers several key advantages: it reduces circuit depth, minimizes the use of multi-qubit gates, and efficiently allocates quantum resources, capabilities that are essential for overcoming the noise limitations of current NISQ-era hardware. Furthermore, by explicitly incorporating realistic noise effects, including laser intensity noise and phase noise, our simulations demonstrate that high-fidelity variational compilation can still be maintained. This confirms the strong noise resilience of the scheme and its suitability for near-term quantum devices. By performing quantum compilation directly through native gates, the method provides significant benefits for quantum simulation on NISQ hardware. We believe our work can further enhance the utility of near-term quantum devices and can be extended to the simulation of strongly correlated electronic systems and non-equilibrium quantum dynamics.

Appendix A: The Hamiltonian of the hydrogen chain

We have simulated the Hamiltonians of H_2, H_3, and H_4 as follows. The hydrogen H_2 molecule consists of two hydrogen atoms. At its equilibrium configuration, it is a linear diatomic molecule, with the two nuclei positioned along the z-axis and a bond length of 0.7414 Å. In a three-dimensional Cartesian coordinate system (x, y, z), the coordinates of the two hydrogen atoms are given as (0.0, 0.0, 0.0) and (0.0, 0.0, 0.7414). Based on this geometry, the electronic Hamiltonian of the molecule is obtained via the second-quantization formalism and then mapped onto a sum of Pauli operators acting on qubits using the Jordan–Wigner transformation. The H_2 qubit Hamiltonian is

$$\begin{aligned} H_{H_2} = &-0.09886396933545849I + 0.17119774903432994Z_0 + 0.17119774903432994Z_1 \\ &- 0.2227859304041847Z_2 - 0.2227859304041847Z_3 + 0.1686221915892095Z_0Z_1 \\ &+ 0.12054482205301797Z_0Z_2 + 0.165867024105892Z_0Z_3 + 0.165867024105892Z_1Z_2 \\ &+ 0.12054482205301797Z_1Z_3 + 0.17434844185575687Z_2Z_3 - 0.045322202052874X_0X_1Y_2Y_3 \\ &+ 0.045322202052874X_0Y_1Y_2X_3 + 0.045322202052874Y_0X_1X_2Y_3 - 0.045322202052874Y_0Y_1X_2X_3. \end{aligned} \tag{A1}$$

For the H_3 molecule, which consists of three hydrogen atoms, we adopt a configuration in which all atoms are arranged linearly along the z-axis. The three hydrogen atoms are equally spaced, with their specific coordinates given as (0.0, 0.0, −0.75),

(0.0, 0.0, 0.0), and (0.0, 0.0, 0.75), exhibiting inversion symmetry. When the STO-3G basis set is chosen and the Jordan–Wigner transformation is applied to map the system onto a qubit Hamiltonian, the qubit Hamiltonian can be written as

$$
\begin{aligned}
H_{\mathrm{H_3}} = {} & 0.2140949245008363I + 0.21477745866084974Z_0 + 0.21477745866084974Z_1 - 0.0065997397459670315Z_2 \\
& - 0.0065997397459670976Z_3 - 0.4498201168785577Z_4 - 0.4498201168785577Z_5 + 0.15479415208426195Z_0Z_1 \\
& + 0.09832339582986878Z_0Z_2 + 0.13687368490017215Z_0Z_3 \\
& + 0.0013038055590903347X_0Z_1Z_2Z_3X_4 + 0.0013038055590903347Y_0Z_1Z_2Z_3Y_4 \\
& + 0.12810230224564145Z_0Z_4 + 0.16029572361892896Z_0Z_5 + 0.13687368490017215Z_1Z_2 + 0.09832339582986878Z_1Z_3 \\
& + 0.16029572361892896Z_1Z_4 + 0.0013038055590903347X_1Z_2Z_3Z_4X_5 \\
& + 0.0013038055590903347Y_1Z_2Z_3Z_4Y_5 + 0.12810230224564145Z_1Z_5 \\
& + 0.14585519030093116Z_2Z_3 + 0.10903856047940377Z_2Z_4 + 0.14494382536401848Z_2Z_5 + 0.14494382536401848Z_3Z_4 \\
& + 0.10903856047940377Z_3Z_5 + 0.17730958056525326Z_4Z_5 \\
& - 0.024565324969942518Z_0X_1Z_2Z_3Z_4X_5 - 0.024565324969942518Z_0Y_1Z_2Z_3Z_4Y_5 \\
& - 0.024565324969942515X_0Z_2Z_3X_4 - 0.024565324969942515Y_0Z_2Z_3Y_4 \\
& - 0.038550289070303355X_0X_1Y_2Y_3 + 0.038550289070303355X_0Y_1Y_2X_3 \\
& + 0.038550289070303355Y_0X_1X_2Y_3 - 0.038550289070303355Y_0Y_1X_2X_3 \\
& - 0.03219342137328751X_0X_1Y_4Y_5 + 0.03219342137328751X_0Y_1Y_4X_5 \\
& + 0.03219342137328751Y_0X_1X_4Y_5 - 0.03219342137328751Y_0Y_1X_4X_5 \\
& - 0.02930007839083853X_0Z_1Z_3X_4 - 0.02930007839083853Y_0Z_1Z_3Y_4 \\
& - 0.033364474660525806X_0Z_1X_2X_3Z_4X_5 - 0.033364474660525806X_0Z_1X_2Y_3Z_4Y_5 \\
& - 0.033364474660525806Y_0Z_1Y_2X_3Z_4X_5 - 0.033364474660525806Y_0Z_1Y_2Y_3Z_4Y_5 \\
& + 0.00406439626968727 7X_0Z_1Z_2X_4 + 0.00406439626968727 7Y_0Z_1Z_2Y_4 \\
& - 0.02586912837359516X_0Z_1Z_2Z_3X_4Z_5 - 0.02586912837359516Y_0Z_1Z_2Z_3Y_4Z_5 \\
& + 0.00406439626968727 7X_1Z_3Z_4X_5 + 0.00406439626968727 7Y_1Z_3Z_4Y_5 \\
& + 0.033364474660525806X_1X_2Y_3Y_4 - 0.033364474660525806X_1Y_2Y_3X_4 \\
& - 0.033364474660525806Y_1X_2X_3Y_4 + 0.033364474660525806Y_1Y_2X_3X_4 \\
& - 0.02930007839083853X_1Z_2Z_4X_5 - 0.02930007839083853Y_1Z_2Z_4Y_5 \\
& - 0.02586912837359516X_1Z_2Z_3X_5 - 0.02586912837359516Y_1Z_2Z_3Y_5 \\
& - 0.03590526488461471X_2X_3Y_4Y_5 + 0.03590526488461471X_2Y_3Y_4X_5 \\
& + 0.03590526488461471Y_2X_3X_4Y_5 - 0.03590526488461471Y_2Y_3X_4X_5. \qquad \text{(A2)}
\end{aligned}
$$

For the H_4 molecule, we adopt a two-dimensional square (planar four-atom) system composed of four hydrogen atoms. All atoms lie in the *xy*-plane, forming a square whose center is at the origin and whose sides are oriented at 45° to the coordinate axes. The specific coordinates are $(0.75, 0.75, 0.0)$, $(-0.75, 0.75, 0.0)$, $(-0.75, -0.75, 0.0)$, and $(0.75, -0.75, 0.0)$, with a nearest-neighbor distance of 1.5 Å. When the STO-3G basis set is chosen and the Jordan–Wigner transformation is applied to map the system onto a qubit Hamiltonian, the qubit Hamiltonian can be written as

$$
\begin{aligned}
H_{\mathrm{H_4}} = {} & -0.8823205468513725I + 0.1472858238295592Z_0 + 0.14728582382955913Z_1 + 0.020729283262210796Z_2 \\
& + 0.020729283262210796Z_3 + 0.020729283262211046Z_4 + 0.020729283262210976Z_5 - 0.10711575592668729Z_6 \\
& - 0.10711575592668729Z_7 + 0.10715401025424172Z_0Z_1 + 0.07213887045360731Z_0Z_2 + 0.10619725547611045Z_0Z_3 \\
& + 0.07213887045360727Z_0Z_4 + 0.10619725547611045Z_0Z_5 + 0.08409543193051364Z_0Z_6 + 0.10718909625701004Z_0Z_7 \\
& + 0.10619725547611045Z_1Z_2 + 0.07213887045360731Z_1Z_3 + 0.10619725547611045Z_1Z_4 + 0.07213887045360727Z_1Z_5 \\
& + 0.10718909625701004Z_1Z_6 + 0.08409543193051364Z_1Z_7 + 0.10799421374369352Z_2Z_3 + 0.08187250448950978Z_2Z_4 \\
& + 0.10617090538145485Z_2Z_5 + 0.07102689631806358Z_2Z_6 + 0.10930666421058499Z_2Z_7 + 0.10617090538145485Z_3Z_4 \\
& + 0.08187250448950978Z_3Z_5 + 0.10930666421058499Z_3Z_6 + 0.07102689631806358Z_3Z_7 + 0.10799421374369343Z_4Z_5
\end{aligned}
$$

$$
\begin{aligned}
&+0.07102689631806 36Z_4Z_6+0.10930666421058491Z_4Z_7+0.10930666421058491Z_5Z_6+0.07102689631806 36Z_5Z_7\\
&+0.11263850647926825Z_6Z_7-0.03405838502250312X_0X_1Y_2Y_3\\
&+0.03405838502250312X_0Y_1Y_2X_3+0.03405838502250312Y_0X_1X_2Y_3\\
&-0.03405838502250312Y_0Y_1X_2X_3-0.03405838502250316X_0X_1Y_4Y_5\\
&+0.03405838502250316X_0Y_1Y_4X_5+0.03405838502250316Y_0X_1X_4Y_5\\
&-0.03405838502250316Y_0Y_1X_4X_5-0.02309366432649641 3X_0X_1Y_6Y_7\\
&+0.02309366432649641 3X_0Y_1Y_6X_7+0.02309366432649641 3Y_0X_1X_6Y_7\\
&-0.02309366432649641 3Y_0Y_1X_6X_7+0.01157311348019658 7X_0Z_1X_2X_4Z_5X_6\\
&+0.01157311348019658 7X_0Z_1Y_2Y_4Z_5X_6+0.01157311348019658 7Y_0Z_1X_2X_4Z_5Y_6\\
&+0.01157311348019658 7Y_0Z_1Y_2Y_4Z_5Y_6-0.03525752032766723 4X_0Z_1Z_2X_3Y_4Z_5Z_6Y_7\\
&+0.03525752032766723 4X_0Z_1Z_2Y_3Y_4Z_5Z_6X_7+0.03525752032766723 4Y_0Z_1Z_2X_3X_4Z_5Z_6Y_7\\
&-0.03525752032766723 4Y_0Z_1Z_2Y_3X_4Z_5Z_6X_7-0.02368440684747064 7X_0Z_1Z_2X_3X_5X_6\\
&-0.02368440684747064 7X_0Z_1Z_2Y_3Y_5X_6-0.02368440684747064 7Y_0Z_1Z_2X_3X_5Y_6\\
&-0.02368440684747064 7Y_0Z_1Z_2Y_3Y_5Y_6+0.03525752032766723 4X_0Z_1X_2X_5Z_6X_7\\
&+0.03525752032766723 4X_0Z_1X_2Y_5Z_6Y_7+0.03525752032766723 4Y_0Z_1Y_2X_5Z_6X_7\\
&+0.03525752032766723 4Y_0Z_1Y_2Y_5Z_6Y_7-0.02368440684747064 7X_1X_2X_4Z_5Z_6X_7\\
&-0.02368440684747064 7X_1Y_2Y_4Z_5Z_6X_7-0.02368440684747064 7Y_1X_2X_4Z_5Z_6Y_7\\
&-0.02368440684747064 7Y_1Y_2Y_4Z_5Z_6Y_7-0.03525752032766723 4X_1X_2Y_5Y_6\\
&+0.03525752032766723 4X_1Y_2Y_5X_6+0.03525752032766723 4Y_1X_2X_5Y_6\\
&-0.03525752032766723 4Y_1Y_2X_5X_6+0.01157311348019658 7X_1Z_2X_3X_5Z_6X_7\\
&+0.01157311348019658 7X_1Z_2Y_3Y_5Z_6X_7+0.01157311348019658 7Y_1Z_2X_3X_5Z_6Y_7\\
&+0.01157311348019658 7Y_1Z_2Y_3Y_5Z_6Y_7+0.03525752032766723 4X_1Z_2X_3X_4Z_5X_6\\
&+0.03525752032766723 4X_1Z_2X_3Y_4Z_5Y_6+0.03525752032766723 4Y_1Z_2Y_3X_4Z_5X_6\\
&+0.03525752032766723 4Y_1Z_2Y_3Y_4Z_5Y_6-0.02429840089194508 5X_2X_3Y_4Y_5\\
&+0.02429840089194508 5X_2Y_3Y_4X_5+0.02429840089194508 5Y_2X_3X_4Y_5\\
&-0.02429840089194508 5Y_2Y_3X_4X_5-0.03827976789252139 6X_2X_3Y_6Y_7\\
&+0.03827976789252139 6X_2Y_3Y_6X_7+0.03827976789252139 6Y_2X_3X_6Y_7\\
&-0.03827976789252139 6Y_2Y_3X_6X_7-0.03827976789252133 4X_4X_5Y_6Y_7\\
&+0.03827976789252133 4X_4Y_5Y_6X_7+0.03827976789252133 4Y_4X_5X_6Y_7-0.03827976789252133 4Y_4Y_5X_6X_7. \qquad \text{(A3)}
\end{aligned}
$$

Data availability statement

The data that support the findings of this study are openly available at https://doi.org/10.5281/zenodo.17199318.

Acknowledgements

This work is supported by the National Natural Science Foundation of China (Grant Nos. 12074433, 12004430, 12174447, and 12174448).

References

[1] Shor P W 1997 *SIAM Journal on Computing* **26** 1484
[2] Feynman R P 1982 *International Journal of Theoretical Physics* **21** 467
[3] Preskill J 2018 *Quantum* **2** 79
[4] Fowler A G 2011 *Quantum Information and Computation* **11** 867
[5] Chong F T, Franklin D and Martonosi M 2017 *Nature* **549** 180
[6] Nam Y, Ross N J, Su Y, Childs A M and Maslov D 2018 *npj Quantum Information* **4** 23
[7] Heyfron L E and Campbell E T 2019 *Quantum Science and Technology* **4** 015004
[8] Duncan R, Kissinger A, Perdrix S and Van De Wetering J 2020 *Quantum* **4** 279
[9] Camps D and Van Beeumen R 2020 *Phys. Rev. A* **102** 052411
[10] Ferrari D and Amoretti M 2018 *International Journal of Quantum Information* **16** 1840006
[11] Cincio L, Subaşı Y, Sornborger A T and Coles P J 2018 *New J. Phys.* **20** 113022
[12] Moro L, Paris M G, Restelli M and Prati E 2021 *Commun. Phys.* **4** 178
[13] Zhang Y H, Zheng P L, Zhang Y and Deng D L 2020 *Phys. Rev. Lett.* **125** 170501
[14] Trenkwalder L M, Scerri E, O'Brien T E and Dunjko V 2023 arXiv:2311.04285
[15] Venturelli D, Do M, Rieffel E and Frank J 2018 *Quantum Science and Technology* **3** 025004

[16] Peruzzo A, McClean J, Shadbolt P, Yung M H, Zhou X Q, Love P J, Aspuru-Guzik A and O'brien J L 2014 *Nat. Commun.* **5** 4213

[17] O'Malley P J, Babbush R, Kivlichan I D, Romero J, McClean J R, Barends R, Kelly J, Roushan P, Tranter A, Ding N, *et al*. 2016 *Phys. Rev. X* **6** 031007

[18] Han H S C, Wang P and Zhang M 2025 *Chin. Phys. B* **34** 120304

[19] Luo T Y and Deng Y X 2026 *Chin. Phys. B* **35** 040309

[20] Wecker D, Hastings M B and Troyer M 2015 *Phys. Rev. A* **92** 042303

[21] Possel C, Hahn W, Shirazi R, Walt M, Pinski P, Wilhelm F K and Bagrets D 2025 arXiv:2505.19772

[22] Anand A and Brown K R 2025 *Phys. Rev. A* **111** 012437

[23] Anand A and Brown K R 2025 *Quantum Science and Technology* **10** 045009

[24] Khatri S, LaRose R, Poremba A, Cincio L, Sornborger A T and Coles P J 2019 *Quantum* **3** 140

[25] Heya K, Suzuki Y, Nakamura Y and Fujii K 2018 arXiv:1810.12745

[26] Gokhale P, Ding Y, Propson T, Winkler C, Leung N, Shi Y, Schuster D I, Hoffmann H and Chong F T 2019 *Proceedings of the 52nd Annual IEEE/ACM International Symposium on Microarchitecture* 266

[27] Jones T and Benjamin S C 2022 *Quantum* **6** 628

[28] Debnath S, Linke N M, Figgatt C, Landsman K A, Wright K and Monroe C 2016 *Nature* **536** 63

[29] H?ffner H, Roos C F and Blatt R 2008 *Phys. Rep.* **469** 155

[30] Martinez E A, Monz T, Nigg D, Schindler P and Blatt R 2016 *New J. Phys.* **18** 063029

[31] Maslov D 2017 *New J. Phys.* **19** 023035

[32] Sch?fer V, Ballance C, Thirumalai K, Stephenson L, Ballance T, Steane A and Lucas D 2018 *Nature* **555** 75

[33] Chen W, Gan J, Zhang J N, Matuskevich D and Kim K 2021 *Chin. Phys. B* **30** 060311

[34] Hempel C, Maier C, Romero J, McClean J, Monz T, Shen H, Jurcevic P, Lanyon B P, Love P, Babbush R, *et al*. 2018 *Phys. Rev. X* **8** 031022

[35] Nam Y, Chen J S, Pisenti N C, Wright K, Delaney C, Maslov D, Brown K R, Allen S, Amini J M, Apisdorf J, *et al*. 2020 *npj Quantum Information* **6** 33

[36] Zhao L, Goings J, Shin K, Kyoung W, Fuks J I, Kevin Rhee J K, Rhee Y M, Wright K, Nguyen J, Kim J, *et al*. 2023 *npj Quantum Information* **9** 60

[37] Khan I, Tudorovskaya M, Kirsopp J, Muñoz Ramo D, Warrier P, Papanastasiou D and Singh R 2023 *J. Chem. Phys.* **158** 214414

[38] Steane A M 1996 *Phys. Rev. Lett.* **77** 793

[39] Sørensen A and Mølmer K 2000 *Phys. Rev. A* **62** 022311

[40] Wang J B 2025 *Chin. Phys. B* **34** 040302

[41] Lu Y, Zhang S, Zhang K, Chen W, Shen Y, Zhang J, Zhang J N and Kim K 2019 *Nature* **572** 363

[42] Georgescu I M, Ashhab S and Nori F 2014 *Rev. Mod. Phys.* **86** 153

[43] Blatt R and Roos C F 2012 *Nat. Phys.* **8** 277

[44] Sun S N, Motta M, Tazhigulov R N, Tan A T, Chan G K L and Minnich A J 2021 *PRX Quantum* **2** 010317

[45] Yuan X, Sun J, Liu J, Zhao Q and Zhou Y 2021 *Phys. Rev. Lett.* **127** 040501

[46] Kitaev A Y 1995 arXiv:quant-ph/9511026

[47] Aspuru-Guzik A, Dutoi A D, Love P J and Head-Gordon M 2005 *Science* **309** 1704

[48] Jordan P and Wigner E 1928 *Zeitschrift für Physik* **47** 631

[49] Bravyi S B and Kitaev A Y 2002 *Annals of Physics* **298** 210

[50] Lloyd S 1996 *Science* **273** 1073

[51] Hastings M B, Wecker D, Bauer B and Troyer M 2014 arXiv:1403.1539

[52] Babbush R, McClean J, Wecker D, Aspuru-Guzik A and Wiebe N 2015 *Phys. Rev. A* **91** 022311

[53] Whitfield J D, Biamonte J and Aspuru-Guzik A 2011 *Molecular Physics* **109** 735

[54] Campbell E 2019 *Phys. Rev. Lett.* **123** 070503

[55] Wan K, Berta M and Campbell E T 2022 *Phys. Rev. Lett.* **129** 030503

[56] Nielsen M A and Chuang I L 2010 *Quantum computation and quantum information* (Cambridge: Cambridge University Press)

[57] Kingma D P and Ba J 2017 arXiv:1412.6980

[58] Ransford A, Allman M S, Arkinstall J, Campora J P, Cooper S F, Delaney R D, Dreiling J M, Estey B, Figgatt C, Hall A, *et al.* 2026 *Nature* **655** 81